Turkish Computational and Theoretical Chemistry

Turkish Comp Theo Chem (TC&TC)

Volume(Issue): 7(2) – Year: 2023 – Pages: 58-69

e-ISSN: 2602-3237

https://doi.org/10.33435/tcandtc.1181299

Received: 28.09.2022 ***Accepted:*** 15.12.2022 *Research Article*

IN SILICO STUDY OF APTAMER SPECIFICITY FOR DETECTION OF ADENOSINE TRIPHOSPHATE (ATP) AS BIOSENSOR DEVELOPMENT FOR MITOCHONDRIA DIABETES DIAGNOSIS

Rustaman Rustaman, Rizky Rafi Rahmawan, Iman Permana Maksum[1]

Departement of Chemistry, Faculty of Mathematics and Natural Sciences, Padjadjaran University, Bandung, Indonesia

Abstract: Diabetes Mellitus (DM) is characterized by increased blood glucose levels. It is generally caused by the pancreas' inability to produce insulin due to cell damage or insulin resistance. Due to the inhibition of adenosine triphosphate (ATP) production, which is essential for insulin secretion, one clinical pathology of this complication is insulin secretion dysfunction. Common methods of blood sugar diagnostics cannot distinguish mitochondrial diabetes and can lead to medication errors. Furthermore, an approach was developed through ATP biomarkers using an electrochemical biosensor with the help of an aptamer. However, it remains unknown precisely how and where the molecular interactions between the modified aptamer and ATP occur. Simulations were conducted in this study for 100 ns in silico using the amber18 computer program to determine the stability of the interaction and specificity between aptamer-ATP were compared to ADP and AMP. The results showed that the significant interactions are three hydrogen bonds between ATP and G7, G8, and A24. It was discovered that the aptamer-ATP complex had moderately good interaction and better potential for specificity than ADP and AMP. According to the RMSD, RMSF, and binding energy profiles, the system is still searching for the best conformation, necessitating a longer simulation time and additional studies to optimize the system. As a result, the system can reach a stable state and determine a more accurate energy calculation, hence, it is interpreted according to real applications.

Keywords: Aptamer; ATP; Mitochondrial diabetes; In Silico; Molecular Dynamic Simulation.

1. Introduction

Diabetes Mellitus (DM) is a disease that occurs due to the disruption of glucose metabolism in cells, leading to an increasing concentration of glucose in the blood or hyperglycemia. In 2021, the number of sufferers recorded by the International Diabetes Federation (IDF) was 537 million adults aged 20-79. Furthermore, it implies that 1 in 10 people have this disease worldwide. This disease also kills about 6.7 million individuals yearly, which is analogous to the prevalence of death that reaches 1 person every 5 seconds. The incidence continues to increase and even tends to be alarming. Diabetes Mellitus can cause eye, heart, nerves, and kidney complications, leading to amputation. This is a very severe disease, hence, it is called a silent killer by many experts [1].

Diabetes Mellitus is generally divided into type 1 and type 2. The first occurs when the pancreas cannot produce insulin due to cell damage, while in the second, insulin is produced normally but increases blood sugar levels due to impaired regulation. Mitochondrial diabetes is a type 2 DM caused by dysfunction of insulin secretion due to inhibition of adenosine triphosphate (ATP) production. This dysfunction is related to mutations in mitochondrial genes [2].

Diabetes Mellitus is diagnosed by measuring blood sugar levels. The diagnosis of type 2 diabetes was conducted using the glycated hemoglobin (HbA1c)

[1] Corresponding Authors

e-mail: iman.permana@unpad.ac.id

test. This shows the average blood sugar and hemoglobin level over the past two to three months. It is concluded that the patient has this disease when the HbA1c level is above 6.5% [3]. Furthermore, ATP can be used as a biomarker to detect mitochondrial diabetes caused by the A3243G mutation.

Adenosine triphosphate (ATP) is essential in many biological processes, such as regulating cellular metabolism and biochemical pathways [4]. Most mitochondrial diseases arise due to disturbances in the process of oxidative phosphorylation. The vital role of mitochondria in producing energy in the form of ATP is disrupted when this process is inhibited, resulting in cellular abnormalities and cell death [5]. Previous studies stated that Diabetes Mellitus and cataracts are caused by mutations occurring in the respiratory complex [6-7]. There is a prospect that the development of aptasensor application diagnostic methods can strengthen previous in vitro and silico studies on mitochondrial DNA mutation [8-10]. Particularly, the A3243G mutation in the leucine tRNA leads to the formation of a dimer that interferes with its biomolecular function. The conformational energy and RMSD values for intermolecular interactions indicate that the structure of mutant leucine tRNA dimers is more stable than its normal counterpart, which has fewer intermolecular hydrogen bonds [11].

The importance of studying mitochondrial diabetes is related to the different ways of treatment with other types 2 DM, which include administration of insulin, oral drugs to increase insulin secretion (sulphonylurea), Q10 to improve respiratory function, or administration of antioxidant supplements. Therefore, it is necessary to develop appropriate diagnostic methods to determine this disorder.

Advanced alternative diagnostic methods and accurate detection of mitochondrial diabetes are required to obtain the proper treatment. Various techniques for detecting ATP, such as high-performance liquid chromatography (HPLC), mass spectrometry, fluorometric, chemiluminescence, and electrochemical methods, have been developed [12-18]. Among these various techniques, electrochemical sensors are more attractive in development because of their sensitivity, miniaturization ability, low cost, and high stability [19].

The electrochemical biosensor proposed in this study uses an aptamer bioreceptor, hence, it is called an aptasensor. Aptamers are oligonucleotides or short pieces of single-stranded DNA/RNA molecules that recognize specific target molecules. The aptamer was chosen because of its excellent characteristics as a bioreceptor. This implies that it has an excellent affinity for biosensors and other applications, such as biomedical imaging, targeted drug delivery, and biomarker discovery [20].

In 2013, Kashefi-Kheyrabadi developed an electrochemical biosensor based on aptamers conjugated with gold nanoparticles to detect ATP and produce good results [21]. However, because this study was conducted in vitro, it cannot provide information about interactions, specificity, or compatibility between aptasensors and targets. Most known aptamers exhibit a relatively high affinity for adenine but not for sugar and triphosphate groups. They also show a similar affinity for ATP, ADP, and AMP [22]. As a result, further research should be conducted in silico to determine the interaction of the candidate aptasensor with its target, namely ATP, through the interaction site, interaction stability, and efforts to increase the potential of the aptasensor as a diagnosis of mitochondrial diabetes mellitus which can then be applied as a molecular test in health facilities.

2. Computational Method

2.1. Equipment And Materials

The tools and materials for this study are computers to analyze the sequence of aptamers, modeling of aptamer and ATP, as well as their analog molecules, namely ADP and AMP, using several databases and software. Molecular interactions are studied based on anchoring and molecular dynamics using licensed or free access.

2.2. Aptamer and ligand structure preparation

The ssDNA ATP-Binding Aptamer (ABA) sequence with a length of 27 bp [5'-ACC TGG GGG AGT ATT GCG GAG GAA GGT-3'] [14] was obtained from the Research Collaboratory for Structural Bioinformatics (RCSB) Protein Data Bank (PDB) web server with ID PDB: 1AW4. The model obtained from the database does not fully match the required aptamer sequence. According to Kashefi, 2013 ATP-Binding Aptamer was

fragmented at the T13/T14 position into 2 ssDNA fragments. Fragmentation aims for biosensor signaling purposes and leads to the formation of a "sandwich assay" ligand-receptor complex where the condition of the ligand is flanked by the receptor, which is expected to be more stable. Subsequently, each fragment was modified for biosensor signaling purposes. Fragment 1, consisting of the sequence 1-13 [5'-ACC TGG GGG AGT A-3'], was modified at the 5' end by the addition of hexane (CH2)6 and thiol (SH) molecules. The molecule (CH2)6 acts as a linker, and the thiol group at the end of the linker binds the aptamer into gold nanoparticles (AuNP) by coordinating covalent interactions [23], however, AuNP was not added to this study. Fragment 2, consisting of the sequence 14-27 [5'-TT GCG GAG GAA GGT-3'], was modified at the 3' end by the addition of ethane (CH2)2 and amine (NH3) molecules. The NH3 group is added as the signal side of the biosensor. Finally, all modifications are made to the Biovia Discovery Studio application. Molecule structure for ligands used in this study, that is ATP, ADP and AMP also generated in Biovia Discovery Studio application generator, then minimized the structure energy to reach more stable conformation.

2.3. Interaction analysis based on molecular anchoring

The AutoDockTools software is used to study the molecular docking of ATP to wt aptamers and individual fragments by blind docking according to the location of the original ligand, then analyzing the results by examining their energy profiles and interactions.

2.4. Interaction analysis based on molecular dynamics

Licensed software is used for bioinformatics study of ATP molecular dynamics and its analogs with aptamers for 100ns, then analyzing simulation results by examining energy and interaction profiles.

3. Results and discussion

The stability of the interaction against several possible schemes in the system was determined as it consists of more than 2 molecules, intact docking aptamer 1AW4, fragment 1, and fragment 2. In addition to blind docking and site-specific docking procedures, the relevance of the silico test results regarding the selection of an active site is compared with previous studies. Furthermore, 20 complex conformations were formed due to docking Autodock4, and the structure with the lowest energy marked conformation is selected as the outcome

Table 1. List of Interaction ATP with Aptamer

Docking Type	Aptamer	Energy (kcal/mole)	Interaction
Blind docking	wt. aptamer	- 8.92	12 Hydrogen bonds 4 Electrostatics 5 Hydrophobics
	F1	- 4.62	8 Hydrogen bonds 3 Electrostatics
	F2	- 4.57	7 Hydrogen bonds 1 Electrostatic
Specific site docking	wt. aptamer (G9 site)	- 3.81	11 Hydrogen bonds
	wt. aptamer (G22 site)	- 4.12	9 Hydrogen bonds 2 Electrostatics
	F1 (G9)	- 5.59	6 Hydrogen bonds 2 Electrostatics
	F2 (G22)	- 4.76	11 Hydrogen bonds 2 Electrostatics

The docking results display conformational cluster data from the smallest based on the energy rating. The aptamer with ATP obtains a conformation with an average energy of

approximately -5 kcal/mole with quite strong interactions, making it suitable for docking between various conditions. The results showed that the interaction of ATP is quite good with the selected aptamer. The best outcome obtained intact aptamer 1aw4 and F1 with energies of -8.92 kcal/mole and -5.59 kcal/mole, respectively, based on blind docking and specific docking site. The intact aptamer obtains the lowest energy due to many hydrogen bonds. This is in line with the test flow, which requires the two aptamer fragments to interact better with ATP. F1 is considered capable of providing the most significant contribution because it has a more stable interaction than others on its active site.

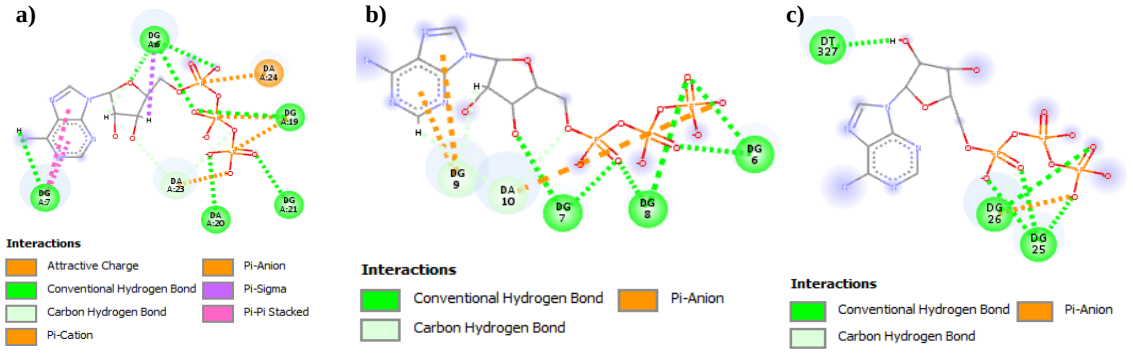

Figure 1. Visualization of Docking conformation. Blind Docking results are shown in pictures a) wt. aptamer-ATP. b) F1-ATP. c) F2-ATP.

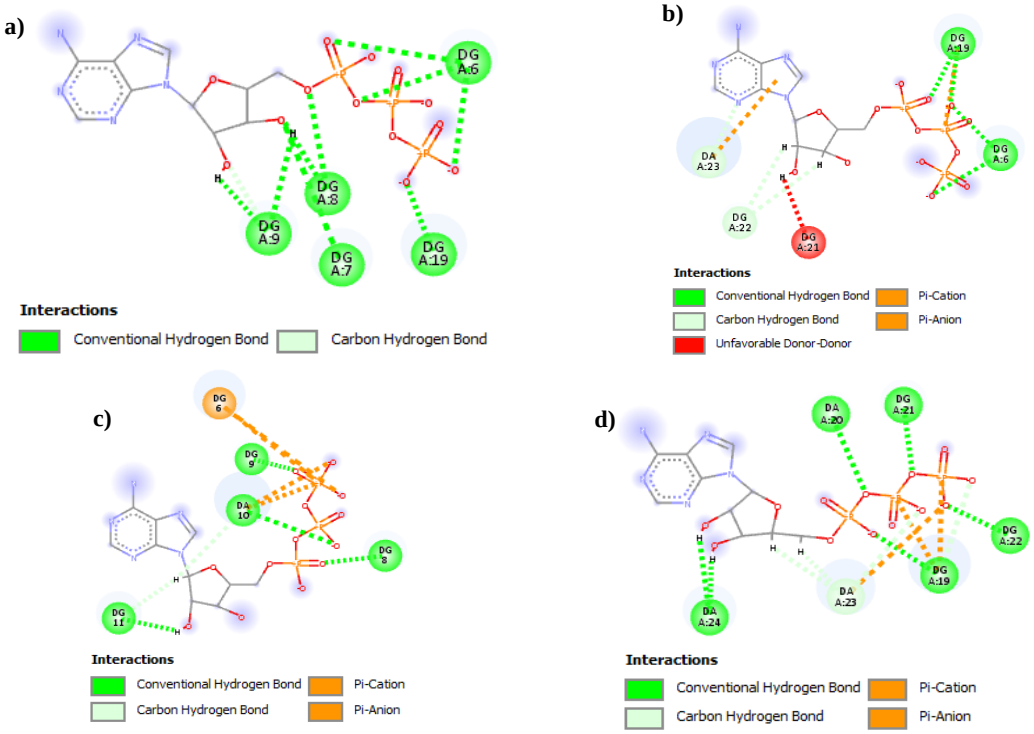

Figure 2. Visualization of Docking conformation. Specific Site Docking is shown in pictures a) wt. aptamer(G9)-ATP. b) wt. aptamer(G22) –ATP. c) F1(G9)-ATP. d) F2(G22)-ATP

The figure shows that the aptamer is a polyanion originating from the phosphodiester backbone, hence it has a negative charge that interacts with ATP on an electropositively charged atom.

Conversely, the surrounding atoms tend to be electropositive when a charge is more electronegative, hence, they can interact with the negative side of ATP. The aptamer still interacts around negatively charged atoms, causing an unfavorable interaction in the form of electrostatic repulsion. This can be explained because these aptamers interact with ATP by electrostatic interactions and their structural complementarity.

The aptamer residues, such as G6, G7, G19, A20, G21, A23, and A24, play a role in the blind docking of ATP to intact aptamer (1AW4). This was compared to docking aptamer F1, namely G6, G7, G8, G9, A10, and F2, including G25, G26, and T27. Furthermore, in the dock site-specific ATP, the intact aptamer (1AW4) sites (G9) are G6, G7, G8, G9, and G19. The intact aptamers at the docking location (G22) are G6, G19, G21 (unfavorable), G22, and A23. The F1 aptamer fragment includes G6, G8, G9, G10 and, G11, while the F2 aptamer fragments are G19, A20, G21, G22, A23, A24.

It was observed that the guanine base contributes significantly to the interaction. Part of its structure also contains adjacent polyguanine, which can form a G-quadruplex that wraps around the ligand with a reasonably strong interaction [24-25]. However, at the docking stage, the conformation of the G-quadruplex could not be confirmed, hence it was continued with molecular dynamics simulation. Hydrogen bonding occurs mainly from the electro-negative atom of the aptamer to the electropositive hydrogen on the sugar group as well as the P and O atoms on the phosphate group of ATP. This is thought to cause ATP testing using aptamers to pose the challenge of interfering with the analyte like other electrostatic species.

A hydrogen bond will occur when the distance between the hydrogen and the electronegative atom is within a radius of less than 3.5. This contributes significantly to the binding affinity of the aptamer-ligand because it is the strongest intermolecular interaction. Furthermore, hydrogen bonding is an electrostatic interaction between hydrogen atoms and oxygen, nitrogen, or fluoride.

These unfavorable interactions are steric and occur between the bases of the aptamer and the ligands. In addition to steric, they can also be in the form of repulsion of atoms with the same positive and negative charge. More unfavorable interactions indicate instability of the aptamer-ATP complex.

The docked aptamer-ATP complex was subjected to molecular dynamics simulations to observe its interactions stability for 100 ns. The simulated system is a fragmented aptamer, namely F1, F2, and ATP, as well as a second phage aptamer system with analogs of ADP and AMP. The complex molecule format is set using the pdb4amber program, hence, it can be recognized by molecular dynamics simulation applications, which are included in the jump program. Parameterization was performed using the force field leaprc.DNA.OL15 for DNA aptamers, leaprc.gaff2 for ligands, and leaprc.tip3p for explicit water in complexes [26–28]. Additionally, Molecular dynamics simulation was conducted for 100 ns with the Amber18 program through several stages, including minimization, heating, equilibration, and production, using a CUDA GPU [29-31].

Table 2. Hydrogen bonding table

Acceptor	Donor H	Donor	Frames	Fraction	Average distance (Å)	Average angle (°)
DG_26@OP1	DG_7@H1	DG_7@N1	1956	0.39	2.82	156.55
DG_17@OP2	DT3_15@HO3'	DT3_15@O3'	1677	0.34	2.66	165.51
DA_24@N3	**ATP_30@HO2'**	**ATP_30@O2'**	**1322**	**0.27**	**2.80**	**163.80**
DA_25@O3'	DG_7@H21	DG_7@N2	950	0.19	2.89	158.52
ATP_30@O2A	**DG_7@H22**	**DG_7@N2**	**665**	**0.13**	**2.86**	**154.54**
DA_24@N3	**ATP_30@HO3'**	**ATP_30@O3'**	**638**	**0.13**	**2.76**	**162.19**
DT3_15@O4	DC_18@H41	DC_18@N4	605	0.12	2.84	163.40
DG_8@OP2	**ATP_30@HN61**	**ATP_30@N6**	**536**	**0.11**	**2.88**	**159.55**
DG_8@OP2	**ATP_30@HN62**	**ATP_30@N6**	**514**	**0.10**	**2.86**	**159.06**

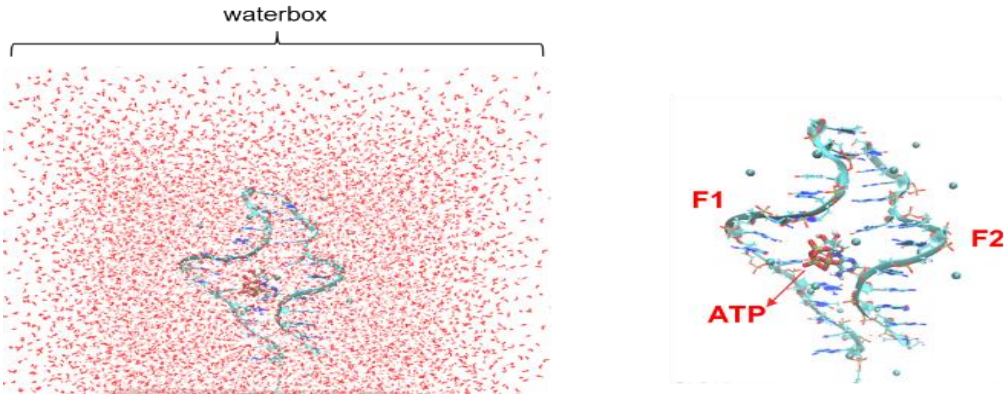

Figure 3. System conformation before simulation.

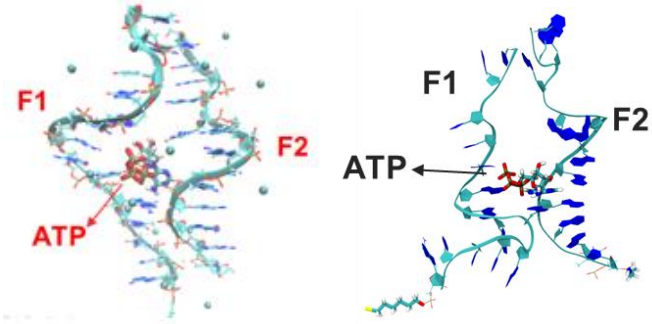

Figure 4. Aptamer-ATP conformation. a) before simulation b) result after simulation for 100ns.

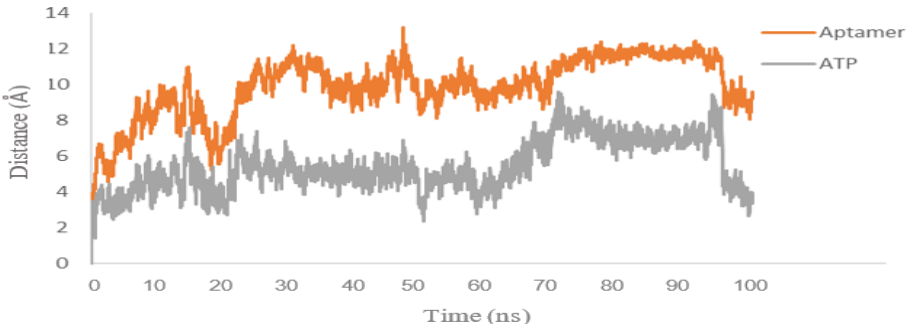

***Figure 5.** RMSD graph for 100ns for aptamer and ATP.*

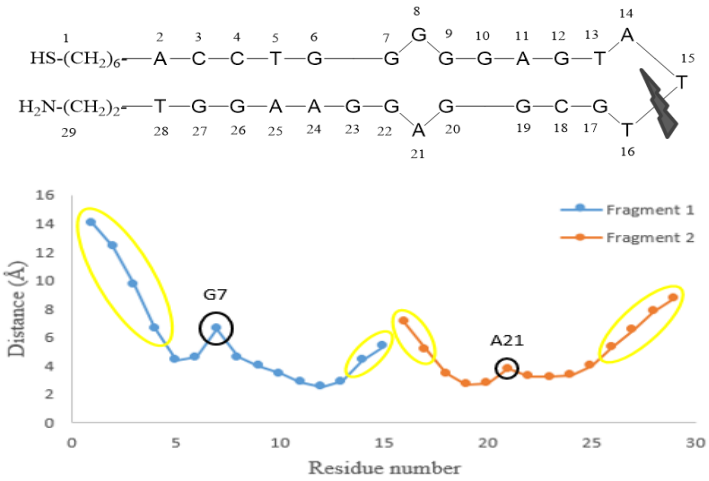

***Figure 6.** a) Visualization after simulation with the residual number. Number 1 and 29 is modified linker in aptamer. b) RMSF graph of aptamer.*

There are several parameters used to analyze the results of molecular dynamics simulations that have been conducted. These include observing the trajectory visually, molecular movement using RMSD and RMSF, hydrogen interaction because it is the strongest, and binding energy using CPPTRAJ [32].

The results of the RMSD aptamer analysis are shown in gray, while ATP is in orange. The aptamer started to increase for both fragments from 0 to approximately 10 Å from the start of the simulation to 16 ns. Subsequently, it drops to 6 Å and rises to 10 Å at 20 ns. The movement is relatively steady at about 10-12 Å from 20 to 95 ns but decreases substantially at 8 Å after 100 ns. Meanwhile, ATP experienced a smaller increase to 5 Å from the beginning of the simulation to 60 ns. It rose sharply near the aptamer shift to 8 Å at 60-95 ns and then decreased along with the movement to 3 Å until the end of the simulation.

The simulation's trajectory visualization confirmed this data, revealing the aptamer's movement in determining the optimal position to interact with each fragment. Because the initial position refers to the docking coordinates, the other side that is not considered is searching for its position during the simulation. On the RMSD chart, it is observed that the movement is still ongoing, indicated by the value, which is quite fluctuating. For ATP molecules, the movement that occurs is mostly the vibration of each atom to obtain the distance between those with the best interaction, and the shift is in line with that of the aptamer. Furthermore, this is indicated by a movement value pattern similar to its aptamer, which is considered sufficient to "lock" the ATP molecule. Therefore, the value of the movement that occurs is relatively small for the flexible ssDNA molecule category.

In the F1 aptamer fragment, residue 1 experienced the most significant movement of 14 Å, presumably because it is the end part, and there are no other stabilizing/complementing molecules. The residues A2, C3, and C4 moved relatively large, presumably influenced by the free-moving end of 1. The G7 residue experienced a slightly greater movement of up to 6-7 Å than the adjacent residue, presumably due to the interaction with ATP molecules. Furthermore, others move quite small in the 3-5 Å range. T15, T16, and G17 also experienced a relatively high movement because each fragment's end resulted from the aptamer's fragmentation, making it move more freely. The slightest visible movement for the F2 aptamer fragment is that the A21 residue is larger than its adjacent counterpart. Similarly to G7, the position/location of residues interacts with ATP. The movement is observed to be greater at residues G29 to 29 because it is the end of the aptamer. The RMSF analysis shows that residues G7 and A21 move larger or more flexibly than others as ATP-binding pockets.

The following table represents the hydrogen bonding interactions during the 100 ns simulation, with a presence percentage of approximately 10% and above. Hydrogen bonds can be observed between the two aptamer fragments and between ATP, F2, and F1 aptamer fragments. The hydrogen bond with a presence of 10% or more is considered significant in a simulation. According to these results, a significant interaction between the aptamer and ATP occurred at residues G7, G8, and A24. For the F1 fragment at the

G7 residue, the interaction occurs between the hydrogen from the guanine base and the O from the sugar group. Also, the interaction for the G8 residue occurs between the oxygen from the phosphate backbone and the 2 hydrogens from the adenine base ATP. The A24 residue interaction for the F2 fragment occurs between the nitrogen of the adenine aptamer base and the hydrogen of the hydroxy sugar group. It can be observed that the majority of interactions take place in the sugar and nitrogen base groups of the ATP.

Table 3. Energy table of the simulation system.

Energy Total (kcal/mole)	Average	Std. Deviation	Std. Error Average
Complex	-6,035.29	27.17	3.00
Receptor	-5,229.33	24.51	2.71
Ligand	-869.53	5.92	0.65
Binding Energy	63.58	7.67	0.85

When observing the analyzed energy components, the positive binding energy is predicted to occur because of the component with a large enough influence, such as the electrostatic energy. This electrostatic energy has a relatively large positive value upon further observation due to the repulsion of electrostatic atoms of similar charge. Specifically, this interaction is between the backbone aptamers and the phosphate groups on ATP.

The ADP and AMP ligands are simulated using the same aptamer to compare their effective interaction with ATP. This was conducted with the belief that the aptamer has better interaction with ATP than ADP and AMP, hence, having better specificity in silico. The specificity is important because of its role in the test as a diagnostic method that should be accurate without the presence of other interfering substances being detected.

Compared to the ATP-Aptamer molecular dynamics simulation, the entire modeling, preparation, and manufacturing process was conducted identically to ensure data coherence. The data for RMSD, RMSF, Hydrogen Bonds and Energy Bonds are displayed below.

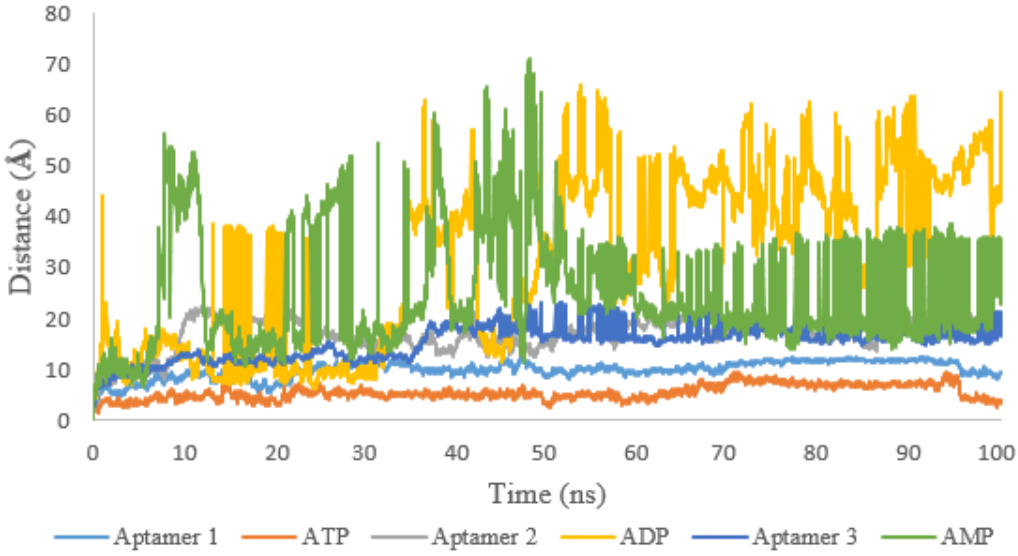

Figure 7. RMSD profile between simulation time and molecular movement. Aptamer 1 is the aptamer in the ATP system, Aptamer 2 is the aptamer in the ADP system, and Aptamer 3 is the aptamer in the AMP system.

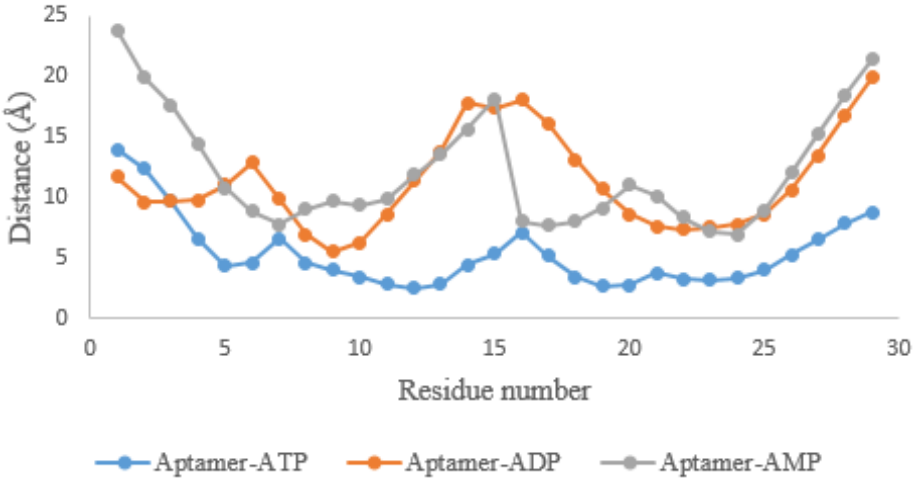

Figure 8. *RMSF profile of the movement of each aptamer base residue during the simulation.*

Aptamer-ATP exhibits less movement than ADP and AMP, as measured by the RMSD value, which indicates how frequently and far the molecule moves relative to its original coordinates. Especially for the ADP and AMP ligands, there is quite a "wild" movement of up to 60 molecules from their initial position. Afterward, the stability of an aptamer-ligand complex can be observed from its movement fluctuations. The Aptamer-ATP system shows a more constant value (not fluctuating) than the others, as shown on the RMSD graph, which tends to be flat with a fairly small movement. The RMSD results show that the aptamer-ATP complex has better stability than ADP and AMP.

The RMSF parameter measures how far the average molecular movement for each aptamer base residue deviates from its initial coordinates. This value helps to determine the base residue with the most significant effect. It can be observed that the residue in Aptamer-ATP has a lower movement than ADP and AMP. For aptamers treated with ADP and AMP ligands, a significant molecular movement occurs up to about 20 from its initial position. This is in line with the RMSD value where Aptamer ADP and AMP move very freely. The results showed that the aptamer-ATP complex has better stability than ADP and AMP.

Table 4. List of hydrogen bonds that occur during the 100ns simulation in the Aptamer-ADP (top) and Aptamer-AMP (bottom) systems.

Acceptor	Donor H	Donor	Frames	Fraction	Avg Distance (Å)	Avg Angle
DT3_15@O4'	DT5_16@HO5'	DT5_16@O5'	185	0,037	2,853	156,1302
ADP@O1B	DG_6@H1	DG_6@N1	142	0,0284	2,8415	155,3871
ADP@O1B	DG_6@H21	DG_6@N2	120	0,024	2,8351	154,9192
ADP@N7	DG_27@H22	DG_27@N2	53	0,0106	2,9141	164,7239
ADP@N1	DG_27@H22	DG_27@N2	52	0,0104	2,9059	164,392
DT_28@O4'	ADP@H62	ADP@N6	50	0,01	2,8738	149,4828

Acceptor	Donor H	Donor	Frames	Fraction	Avg Distance (Å)	Avg Angle
DA_2@OP2	DG_27@H1	DG_27@N1	1293	0,2586	2,826	160,3789
DT3_15@O4	DG_19@H1	DG_19@N1	1021	0,2042	2,8428	149,9994
DA_21@OP2	DG_12@H21	DG_12@N2	986	0,1972	2,8323	157,3256
DT3_15@O2	DG_23@H1	DG_23@N1	964	0,1928	2,8352	155,1326
DG_22@O6	DT3_15@H3	DT3_15@N3	961	0,1922	2,8515	160,9074
AMP@N1	**DG_7@H22**	**DG_7@N2**	**957**	**0,1914**	**2,9026**	**161,6018**
DA_2@OP1	DG_26@H1	DG_26@N1	925	0,185	2,8335	155,0074
DT3_15@O4	DG_19@H21	DG_19@N2	757	0,1514	2,8613	149,1912

Table 5. The calculated binding energy during the 100 ns simulation of Aptamer-ADP (top) and Aptamer-AMP (bottom) systems.

Total Energy (kcal/mole)	Average	Std. Deviation	Std. Error Average
Complex	-5,952.0981	31.3339	3.1334
Reseptor	-5,304.446	26.6768	2.6677
Ligand	-665.1941	4.7218	0.4722
Binding Energy	17.542	9.5526	0.9553

Total Energy (kcal/mole)	Average	Std. Deviation	Std. Error Average
Complex	-5,501.6304	29.8783	2.9878
Reseptor	-5,293.621	29.0667	2.9067
Ligand	-215.1267	4.5238	0.4524
Binding Energy	7.1172	3.3908	0.3391

Hydrogen bonding is widely observed in the interaction of organic compounds or biomolecules because it is the strongest. Therefore, it is significant in determining the stability of the

interaction between 2 or more molecules. Hydrogen bonds that are "considered" significant in molecular dynamic simulations have an interaction percentage above 10% (fraction above 0.1). In this bond, 5 interactions occurred between Aptamer-ATP during the 100 ns simulation. Meanwhile, there are many interactions in Aptamer-ADP, but the percentage is below 3%, which is very small. In Aptamer-AMP, there is only 1 significant hydrogen bond between the N base in AMP and G7 in the aptamer. The remaining Aptamer-AMP system is formed by numerous hydrogen bonds between nitrogenous bases within the aptamer. Based on these data, it is predicted that the aptamer significantly interacts with ATP more than ADP or AMP; this is in line with its RMSD and RMSF values.

Binding energy is a quantitative physical parameter to determine the stability of the complex. The lower the calculated energy, the more stable the simulated system. The three systems give a positive (+) value in this simulation, which indicates that complex systems tend to be less energy stable. Comparing the energy values of the three systems, it is observed that the AMP value is the lowest, followed by ADP and finally ATP. This energy value is inversely proportional to the interpretation of the previous 3 parameters, RMSD, RMSF, and hydrogen bonding. This is due to calculating the energy of complex components involving the energy between the aptamer-aptamer stabilizing interactions. Therefore, the values obtained are slightly "biased." According to the hydrogen bond interactions, it is discovered that there are many hydrogen bond interactions within the Aptamer.

4. Conclusions

These results revealed that the studied fragmented aptamer interacts with ATP during the 100 ns simulation. The significant interactions that occur are the three hydrogen bonds between ATP with G7, G8, and A24. Specifically, the aptamer-ATP complex has fairly good interaction and better potential for specificity than ADP and AMP. Based on the profile of RMSD, RMSF, and their binding energy, the system is still searching for the best conformation, necessitating a longer simulation time and further studies to optimize the system. As a result, the system can reach a stable state and determine more accurate energy calculations, such that it can be interpreted according to real applications.

Acknowledgments

The author is grateful to the Directorate of Research and Community Service (DRPM) Unpad for the RDPD grant (Research Data Library and Online) No. 2203/UN6.3.1/PT.00/2022 and the 2020 Academic Leadership Grant (ALG) No. 1427/UN6.3.1/LT/2020 for funding this research.

References

[1] American Diabetes Association. Diagnosis and classification of diabetes mellitus. Diabetes care. 2011; 34 Suppl 1(Suppl 1), S62–S69.

[2] Kwak, S. H., Park, K. S., Lee, K. U., & Lee, H. K. Mitochondrial metabolism and diabetes. Journal of diabetes investigation. 2010;1(5), 161–169.

[3] Sherwani, S. I., Khan, H. A., Ekhzaimy, A., Masood, A., & Sakharkar, M. K.. Significance of HbA1c Test in Diagnosis and Prognosis of Diabetic Patients. Biomarker insights. 2016; 11, 95–104.

[4] Huang, Y., Lei, J., Cheng, Y., and Ju, H. Target assistant Zn2+-dependent DNAzyme for signal-on electrochemiluminescent biosensing, Electrochim. Acta. 2015;155, 341–347.

[5] Frazier, A.E., Thorburn, D.R., and Compton, A.G. Mitochondrial energy generation disorders: Genes, mechanisms, and clues to pathology, J. Biol. Chem. 2019;294 (14).

[6] Maksum, I.P., Farhani, A., Rachman, S.D., and Ngili, Y. Making of the A3243G mutant template through site directed mutagenesis as positive control in PASA-Mismatch three bases, Int. J. PharmTech Res. 2013;5 (2), 441–450.

[7] Maksum, I.P., Natradisastra, G., Nuswantara, S., and Ngili, Y. The effect of A3243G mutation of mitochondrial DNA to the clinical features of type-2 diabetes mellitus and cataract, Eur. J. Sci. Res. 2013;96 (4), 591–599.

[8] Hartati, Y.W., Nur Topkaya, S., Maksum, I.P., and Ozsoz, M. Sensitive detection of mitochondrial DNA A3243G tRNALeu mutation via an electrochemical biosensor using

Meldola's Blue as a hybridization indicator, Adv. Anal. Chem. 2013;3 (A), 20–27.

[9] Destiarani, W., Mulyani, R., Yusuf, M., and Maksum, I.P. Molecular dynamics simulation of T10609C and C10676G mutations of mitochondrial ND4L gene associated with proton translocation in type 2 diabetes mellitus and cataract patients, Bioinf. Biol. Insights. 2020;14, 117793222097867.

[10] Maksum, I.P., Saputra, S.R., Indrayati, N., Yusuf, M., and Subroto, T. Bioinformatics study of m.9053G>A mutation at the ATP6 gene in relation to type 2 diabetes mellitus and cataract diseases, Bioinf. Biol. Insights. 2017;11, 1177932217728515.

[11] Maksum, I.P., Maulana, A.F., Yusuf, M., Mulyani, R., Destiarani, W., and Rustaman R. Molecular Dynamics Simulation of a tRNA-Leucine Dimer with an A3243G Heteroplasmy Mutation in Human Mitochondria Using a Secondary Structure Prediction Approach. Indonesia J. Chem. 2022;22 (4), 1043-1051.

[12] Khlyntseva, S. V., Y. R. Bazel, A. B. Vishnikin, V. Andruch. Methods for the determination of adenosine triphosphate and other adenine nucleotides, Anal. Chem. 2009;64 657–673.

[13] Huang, Y. F., H. T. Chang. Analysis of adenosine triphosphate and glutathione through gold nanoparticles assisted laser desorption/ionization mass spectrometry. Anal. Chem. 2007;79 4852–4859.

[14] Ning, Y, Wei K., Cheng L. J., Hu J., Xiang Q. Fluorometric aptamer based determination of adenosine triphosphate based on deoxyribonuclease I-aided target recyclingand signal amplification using graphene oxide as a quencher. Microchim Acta. 2017;184:1847–1854.

[15] Liu, XJ, Lin BX, Yu Y, Cao YJ, Guo ML. A multifunctional probe based on the use of labeled aptamer and magnetic nanoparticles for fluorometric determination of adenosine 5′-triphosphate. Microchim Acta. 2018;185:243.

[16] Qu, F., Sun, C., Lv, X. X., You, J. M. A terbium-based metal-organic framework @gold nanoparticle system as a fluorometric probe for aptamer based determination of adenosine triphosphate. Microchim Acta. 2018;185:359.

[17] Srivastava, Priyanka., S.S. Razi, R. Ali, S. Srivastav, S. Patnaik, S. Srikrishna, A. Misra. Highly sensitive cellimaging "Off-On" fluorescentprobe for mitochondria and ATP. Biosens. Bioelectron. 2015;69 179–185.

[18] Chen, J.R., X.X. Jiao, H.Q. Luo, N.B. Li. Probe-label-free electrochemical aptasensor based on methylene blue-anchored graphene oxide amplification, J. Mater. Chem. 2013;B1 861–864.

[19] Yi, Q. and W. Yu. Nanoporous gold particles modified titanium electrode for hydrazine oxidation. J. Electroanal. Chem. 2009;633. 159-164.

[20] Villalonga, A., Pérez-Calabuig, A. M., & Villalonga, R. Electrochemical biosensors based on nucleic acid aptamer. Analytical and Bioanalytical Chemistry. 2020.

[21] Kashefi-Kheyrabadi, Leila and Masoud A. Mehrgard. Aptamer based electrochemical biosensor for detection of adenosine triphos-phate using a nanoporous gold platform. Bioelectrochemistry. 2013.

[22] Nutiu, R., & Li, Y. Structure-Switching Signaling Aptamers. Journal of the American Chemical Society. 2003;123 (16). 4771–4778.

[23] Odeh, F., Nsairat, H., Alshaer, W., Ismail, M. A., Esawi, E., Qaqish, B., … Ismail, S. I. Aptamer Chemistry: Chemical Modifications and Conjugation Strategies. Molecules. 2019;25(1), 3.

[24] Huizenga, David and Jack W. Szostak. A DNA Aptamer That Binds Adenosine and ATP. Biochemistry. 1995;34, 656—665.

[25] Ma, C., Lin, C., Wang, Y., & Chen, X. DNA-based ATP sensing. Trends in Analytical Chemistry. 2016;77. 226-241.

[26] Wang, Junmei & Cieplak, Piotr & Kollman, Peter. How well does a restrained electrostatic potential (RESP) model perform in calculating conformational energies of organic and biological molecules?. Journal of Computational Chemistry. 2000;21. 1049-1074.

[27] Pérez, A., Marchán, I., Svozil, D., Sponer, J., Cheatham, T. E., 3rd, Laughton, C. A., & Orozco, M. Refinement of the AMBER force field for nucleic acids: improving the description of alpha/gamma conformers . Biophysical journal. 2007;92(11).

[28] Zgarbova, M.; Sponer, J.; Otyepka, M.; Cheatham III, T. E.; Galindo-Murillo, R.; Jurecka, P. Refinement of the Sugar–Phosphate Backbone Torsion Beta for Amber Force Fields Improves the Description of Z-and B-DNA. J. Chem. Theory Comput. 2015; 11, 5723–5736.

[29] Romelia Salomon-Ferrer; Andreas W. Goetz; Duncan Poole; Scott Le Grand; Ross C. Walker "Routine microsecond molecular dynamics simulations with AMBER - Part II: Particle Mesh Ewald", J. Chem. Theory Comput. 2013.

[30] Andreas W. Goetz; Mark J. Williamson; Dong Xu; Duncan Poole; Scott Le Grand; Ross C. Walker "Routine microsecond molecular dynamics simulations with AMBER - Part I: Generalized Born", J. Chem. Theory Comput. 2012;8 (5), pp1542-1555.

[31] Scott Le Grand; Andreas W. Goetz; Ross C. Walker "SPFP: Speed without compromise - a mixed precision model for GPU accelerated molecular dynamics simulations.", Comp. Phys. Comm. 2013; 184 pp374-380.

[32] Daniel R. Roe and Thomas E. Cheatham, III, "PTRAJ and CPPTRAJ: Software for Processing and Analysis of Molecular Dynamics Trajectory Data." J. Chem. Theory Comput. 2013;9 (7), pp 3084-3095.